Supplementary Information for

Higher-order Dirac sonic crystals

Huahui Qiu,[1] Meng Xiao,[1] Fan Zhang,[2] and Chunyin Qiu,[1]*

[1]Key Laboratory of Artificial Micro- and Nano-structures of Ministry of Education and School of Physics and Technology, Wuhan University, Wuhan 430072, China

[2]Department of Physics, University of Texas at Dallas, Richardson, Texas 75080, USA

1. Higher-order (HO) topology in a 2D system with C_6 symmetry

Here we briefly review the HO topology of 2D systems with C_6 symmetry[1,2], which can be diagonsed by scrutinizing the irreducible group representations of the bands at high-symmetry points in the 2D hexgonal Brillouin zone, i.e., Γ, M, and K. Specifically, the HO topology of the system can be classified by the topological index $\chi^{(6)} = ([\mathrm{M}], [\mathrm{K}])$, in which the component [M] (or [K]) is a measure of the difference in the C_2 (or C_3) representations at Γ and M (or K). The C_2-invariant $[\mathrm{M}] \in Z$ is defined as $[\mathrm{M}] = \#\mathrm{M}_1 - \#\Gamma_1^{(2)}$, where $\#\mathrm{M}_1$ and $\#\Gamma_1^{(2)}$ count the numbers of negative energy states with C_2 eigenvalue +1 at M and Γ, respectively. Similarly, the C_3-invariant $[\mathrm{K}] \in Z$ is defined as $[\mathrm{K}] = \#\mathrm{K}_1 - \#\Gamma_1^{(3)}$, where $\#\mathrm{K}_1$ and $\#\Gamma_1^{(3)}$ are the numbers of negative energy states with C_3 eigenvalue $+1$ at K and Γ, respectively. The system is topologically nontrivial for a nonzero $\chi^{(6)}$, which is invariant without closing the bulk band gap or breaking the C_6 symmetry. Physically, a nontrivial topological index leads to a fractional charge at the corners of a finite-sized sample: $Q_c = \frac{e}{4}[\mathrm{M}] + \frac{e}{6}[\mathrm{K}] \mod e$, which is a HO manifestation as zero-energy corner modes in the presence of chiral symmetry.

Previous studies[1,2] show that a topological phase transition occurs at $t_0/t_1 = 1$, where the bulk gap closes at Γ point. Specifically, the gapped system is topologically trivial for $t_0/t_1 > 1$, with the bulk index $\chi^{(6)} = (0,0)$ and the coner charge $Q_c = 0$. The system becomes topologically nontrivial for $0 < t_0/t_1 < 1$, with the bulk index $\chi^{(6)} = (\pm 2,0)$ and the corner charge $Q_c = e/2$. Here $\pm$ in the C_2-invariant [M] denote the signs of the inter-cell coupling t_1. Note that in the presence of chiral symmetry the C_3-invariant [K] is always zero since the C_3 operator commutes with the chiral operator[1]. This has also been checked by our calculations.

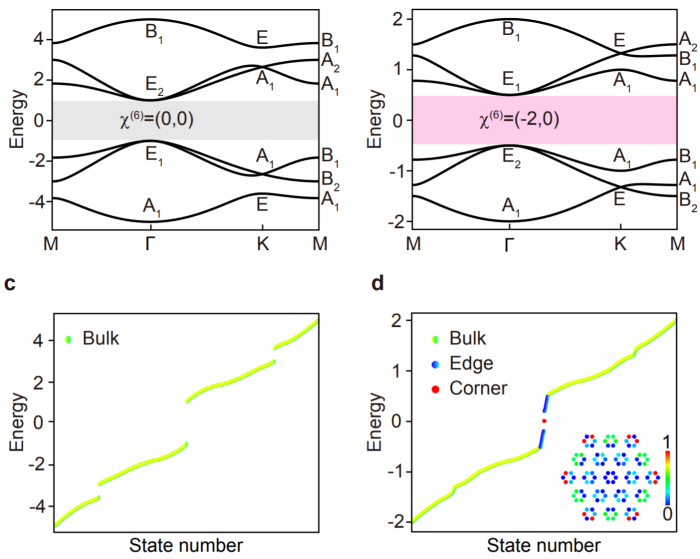

Supplementary Fig. 1 | 2D HO topological insulators with a nontrivial $\chi^{(6)}$ index. a,**b**, Bulk band structures calculated for two different sets of couplings. Irreducible group representations are labeled at the high-symmetry momenta, which give trival and nontrivial $\chi^{(6)}$ indices for these two systems. **c**,**d**, The corresponding corner spectra calculated for finite-sized samples. In contrast to the trival case, the corner spectrum of the nontrivial case exhibits robust corner modes pinned at zero energy (see inset), in addition to the trivial (gapped) edge modes.

Supplimentary Fig. 1 presents two examples to show the HO band topology inherent in the 2D tight-binding model, one for the trvial case ($t_0 = -2$ and $t_1 = -1$) and the other for the nontrivial case ($t_0 = -0.5$ and $t_1 = -1$). After inspecting the eigenstates at the high-symmetry momenta of the three negative energy bands, we can determine the irreducible representations of the C_6 point group and identified the trivial and nontrivial $\chi^{(6)}$ indices for both systems. In contrast to the trivial case, the corner spectrum of the nontrivial case shows clearly robust corner modes pinned at zero energy.

2. Novel 3D HO topological phases predicted by our tight-binding model

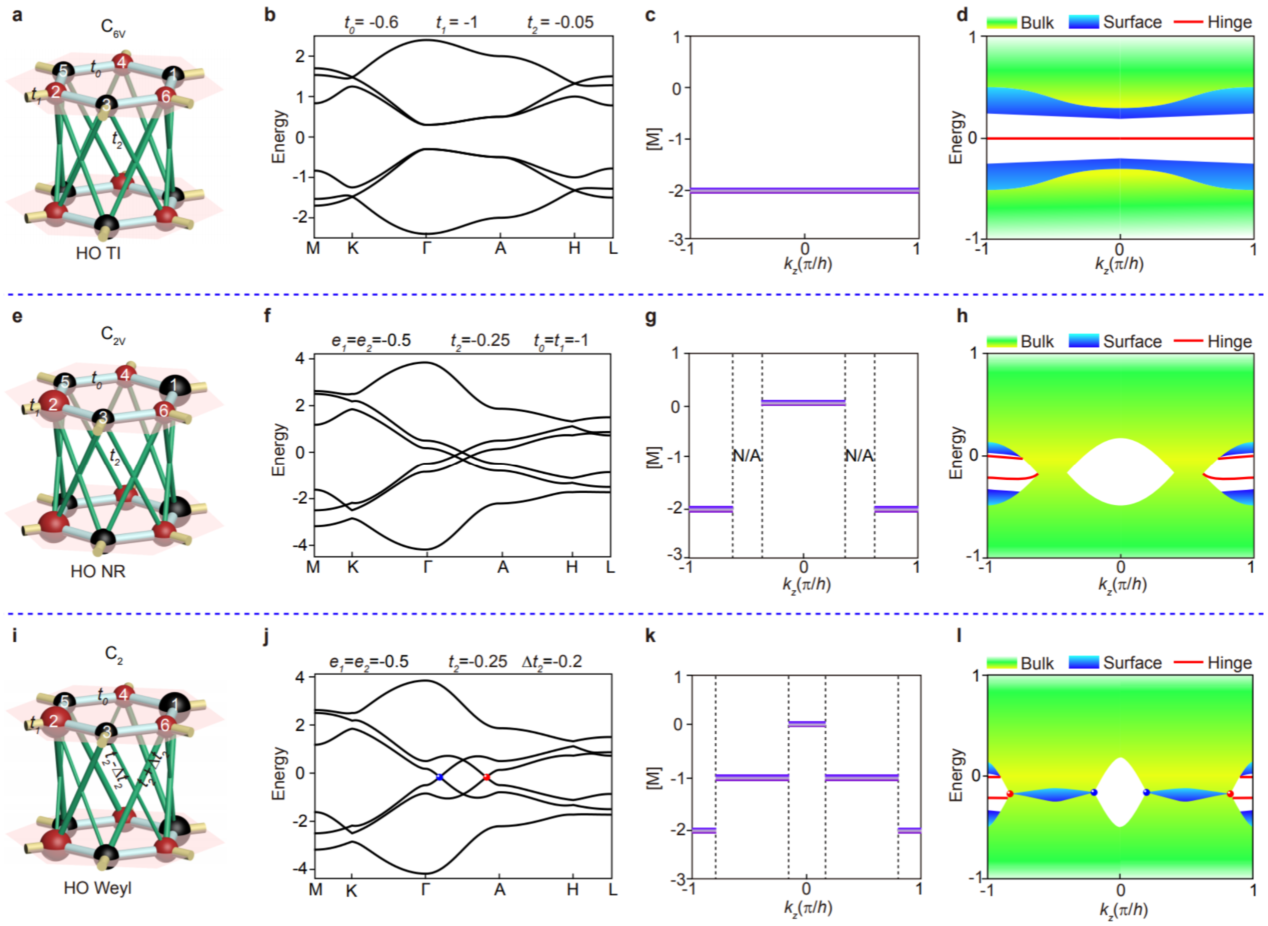

Supplementary Fig. 2 | Novel 3D HO topological phases predicted by our tight-binding model. We focus on the three 3D HO topological phases not discussed in detail in our main text, i.e., HO TI (**a-d**), HO nodal-ring (NR) semimetal (**e-h**), and HO Weyl semimetal (**i-l**). **a**, **e**, and **i** sketch their tight-binding models, **b**, **f**, and **j** plot their bulk band structures, **c**, **g**, and **k** display the k_z-dependent C_2-invariants, and **d**, **h**, and **l** present their hinge spectra. For brievity, the hinge (or surface) states mixing with the projected bulk bands are not presented.

Here we present some numerical details for the three 3D HO topological phases not discussed in detail in our main text (see Fig. 1c), including the HO TI (Supplementary Figs. 2a-2d), HO nodal-ring semimetal (Supplementary Figs. 2e-2h), and HO Weyl semimetal (Supplementary Figs. 2i-2l). As shown in Supplementary Fig. 2a, the HO TI preserves the C_{6v} symmetry but has different couplings compared with the HO Dirac semimetal in the main text. In this case, the hinge spectrum exhibits zero-energy hinge states across the entire hinge Brillouin zone (see Supplementary Fig. 2d), since the same nontrivial C_2-invariant $[\mathrm{M}] = -2$ persists for all k_z (see Supplementary Fig. 2c).

To realize the HO nodal-ring semimetal, we retain the couplings used in the HO Dirac semimetal but add nonzero onsite energies for the sites 1 and 2 ($e_1 = e_2 = -0.5$) to break the C_3 symmetry. In this case, the two double degeneracies in the $\Gamma\mathrm{A}$ line are lifted (see Supplementary Fig. 2f), and each HO Dirac point evolves into a HO nodal ring in the $\Gamma\mathrm{AK}$ mirror plane (see Fig. 2c in the main text). Supplementary Fig. 2g shows the k_z-dependent $[\mathrm{M}]$ index for this C_2-preserved HO nodal-ring system. Comparing with the HO Dirac system (see Fig. 1e in the main text), the k_z distribution of [M] persists outside the k_z region projected by the gapless nodal-ring, in which the C_2-invariant is not well defined. The nontrivial C_2-invariant gives rise to the HO hinge states in Supplementary Fig. 2h, which are no longer pinned at zero energy because of the broken chiral symmetry. The hinge bands split in energy since the six hinges are inequivalent. In addition, the nontrivial surface states responsible for the first-order band topology of nodal rings, which mix with the projected bulk states, are not presented here for brevity. Similarly, the hinge states hidden in the projected bulk (or surface) bands are not displayed, either.

We further break the mirror symmetry in the HO nodal-ring system by assigning different strengths for the clockwise and anticlockwise interlayer couplings ($t_2 \pm 0.2$ used here). Each HO nodal ring evolves into one pair of Weyl points of opposite chirality along the k_z axis (see Fig. 1c in the main text). The hinge states are robust to the perturbation (see Supplementary Fig. 2l), as the hallmark of the HO Weyl semimetal. Interestingly, hybrid band topology occurs within the newly gapped k_z slices between the pair of Weyl points originating from the same Dirac point. The first-order topology is manifested as the nontrivial surface arcs within the corresponding k_z regions (Supplementary Fig. 2l). The HO band topology, related to the nontrivial bulk invariant $[\mathrm{M}] = -1$ in Supplementary Fig. 2k, does not yield well-defined hinge states because of their hybridization with bulk states or surface arcs.

3. Acoustic emulation of the HO Dirac semimetal predicted by our 3D tight-binding model

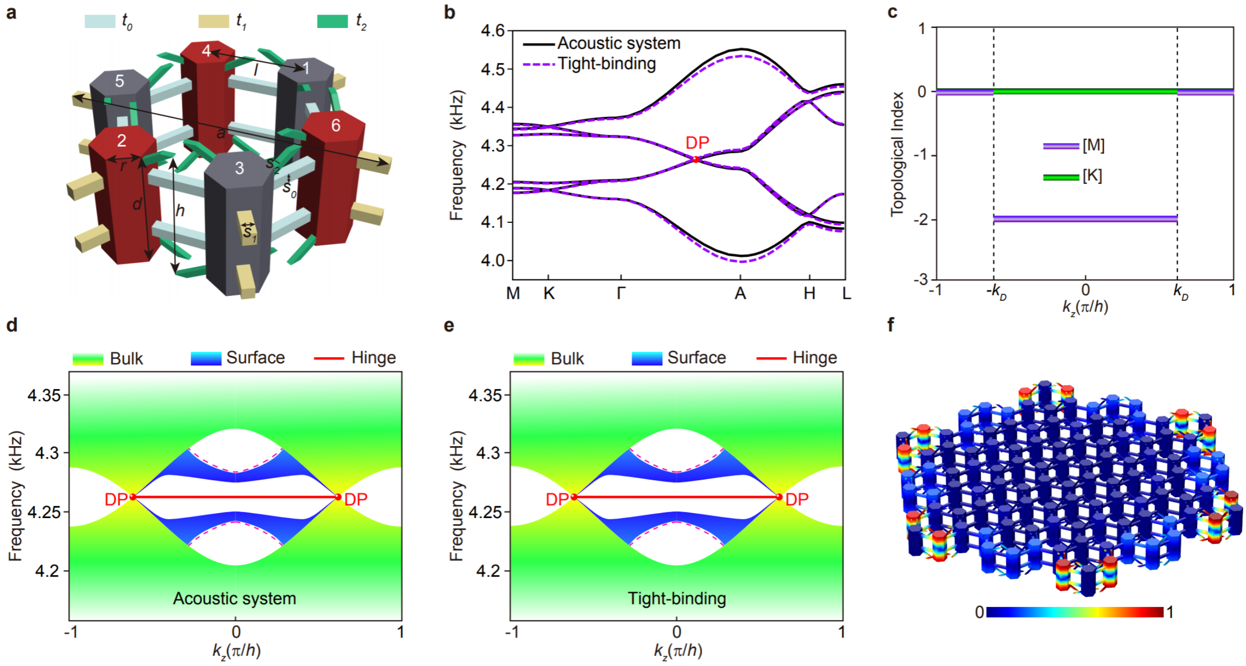

Supplementary Fig. 3 | Direct acoustic emulation of the 3D HO Dirac semimetal. a, Unit cell structure. Physically, the air-filled cavity resonators emulate atomic orbitals, and the narrow tubes introduce couplings between them. **b**, Bulk band structure of the acoustic cavity-tube system, compared with the one fitted by the 3D tight-binding model. The red sphere highlights the Dirac point. **c**, Topological index plotted as a function of k_z, indicating nontrival C_2-invariant ($[M] = -2$) within the momentum range $|k_z| < |k_D|$. **d**, Hinge spectrum simulated for the real acoustic structure, compared with the tight-binding model result in **e**. In addition to the HO hinge states (red solid lines) pinned at zero energy, the system also exhibits topologically trivial hinge states (pink dashed lines). **f**, Simulated eigenfield profile of the hinge modes for the acoustic system, demonstrated with a small sample for clarity.

Here we use an acoustic cavity-tube strcuture to emulate the 3D tight-binding model directly. As shown in Supplementary Fig. 3a, the six (regular hexagonal prism) cavities mimic the orbitals, and the narrow (square) tubes emulate the couplings among them. Specifically, the in-plane and out-of-plane lattice constants are $a = 111$ mm and $h = 45$ mm, respectively. The cavity parameters $r = 10$ mm and $d = 40$ mm are selected to ensure the frequency of the P_z dipole mode ($f_0 = 4264.5$ Hz) to be far away from other cavity modes, serving as a good single-model approximation. This gives the constant onsite energy. The distance between the centers of two neighboring cavity resonators is $l = 37$ mm. Both the intra-cell coupling t_0 and the in-plane inter-cell coupling t_1 are emulated by one pair of horizontal square tubes (located at a distance of $d/2$), with the side-lengths $s_0 = 3.5$ mm and $s_1 = 4.0$ mm. The interlayer coupling t_2 is introduced by the inclined tube of side-length $s_2 = 2.1$ mm. As shown in the Supplementary Fig. 3b, the simulated band structure exhibits clearly fourfold degenerate Dirac points in the ΓA direction. The result is well fitted by the tight-binding model with couplings $t_0 = -56.5$ Hz, $t_1 = -73.5$ Hz, $t_2 = 20.5$ Hz, and $f_0 = 4264.5$Hz. Note that the signs of the couplings are determined by the connectivity of the tubes between the cavities, negative for straight links and positive for inclined links (see Ref. 3 for details). With these couplings, we can derive a nontrivial C_2-invariant ([M] $= -2$) within the momentum range $|k_z| < |k_D|$, as shown in Supplementary Fig. 3c. To identify the HO band topology, we simulate the hinge-projected spectrum for an infinitely long hexagonal prism. As shown in Supplementary Fig. 3d, the HO hinge states, which are flat and pinned at the resonant frequency of the cavity, emerge and connect the pair of projected Dirac points within $|k_z| < |k_D|$, consistent with the k_z-dependent C_2-invariant. In addition to the HO hinge states, the hinge spectrum also exhibits topologically trivial (gapped) surface modes and hinge modes. All these features precisely reproduce the hinge spectrum calculated for the tight-binding model, as shown in Supplementary Fig. 3e. (Note that in contrast to the hinge modes emerging within $|k_z| > |k_D|$ in the main text, here a new set of parameters are used, and the hinge modes appear within $|k_z| < |k_D|$.) The Supplementary Fig. 3f demonstrates the eigenfield profile of the hinge modes simulated for the acoustic system, which is highly-confined to the corners of the sample.

References

1. Noh, J. et al. Topological protection of photonic mid-gap defect modes. *Nat. Photon.* **12**, 408–415 (2018).

2. Benalcazar, W. A., Li, T. & Hughes, T. L. Quantization of fractional corner charge in-symmetric higher-order topological crystalline insulators. *Phys. Rev. B* **99**, 245151 (2019).

3. Qi, Y. et al. Acoustic Realization of Quadrupole Topological Insulators. *Phys. Rev. Lett.* **124**, 206601 (2020).